Inorganic Chemistry

ARTICLE

pubs.acs.org/IC

# A Theoretical Study on the Enhancement of Functionally Relevant Electron Transfers in Biomimetic Models of [FeFe]-Hydrogenases

Claudio Greco* and Luca De Gioia

Department of Biotechnology and Biosciences, Milan-Bicocca University, Piazza della Scienza 2, 20126, Milan, Italy

Supporting Information

**ABSTRACT:** Recent advances aimed at modeling the chemistry of the active site of [FeFe]-hydrogenases (the H-cluster, composed by a catalytic $Fe_2S_2$ subcluster and an $Fe_4S_4$ portion) have led to the synthesis of binuclear coordination compounds containing a noninnocent organophosphine ligand [2,3-bis-(diphenylphosphino)maleic anhydride, bma] that is able to undergo monoelectron reduction, analogously to the tetranuclear $Fe_4S_4$ subcluster portion of the H-cluster. However, such a synthetic model was shown to feature negligible electronic communication between the noninnocent ligand and the remaining portion of the cluster, at variance with the enzyme active site. Here, we report a theoretical investigation that shows why the electron transfer observed in the enzyme upon protonation of the catalytic $Fe_2S_2$ subsite cannot take place in the bma-containing cluster. In addition, we show that targeted modifications of the bma ligand are sufficient to restore the electronic communication within the model, such that electron density can be more easily withdrawn from the noninnocent ligand, as a result of protonation of the iron centers. Similar results were also obtained with a ligand derived from cobaltocene. The relevance of our findings is discussed from the perspective of biomimetic reproduction of proton reduction to yield molecular hydrogen.

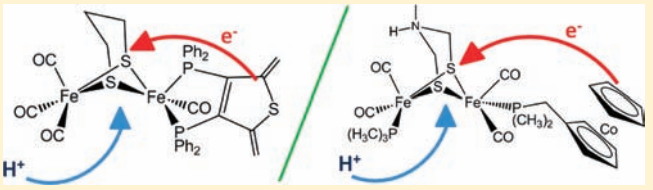


## INTRODUCTION

Electrochemical catalysis of $H_2$ evolution is a key research topic for the development of an oil-free and economically sustainable energy market. Progresses in this area may be achieved by taking as a paradigm the hydrogenases, enzymes that are able to efficiently catalyze the reversible oxidation of molecular hydrogen. In particular, [FeFe]-hydrogenases have attracted attention due to their high catalytic efficiency and due to the presence in their active site of a peculiar iron-containing cofactor. The latter is an $Fe_6S_6$ cluster (the so-called H-cluster, Scheme 1), which can be subdivided into a tetranuclear portion (the $[Fe_4-S_4]_H$ subcluster) and a binuclear subsite ($[2Fe]_H$ in Scheme 1). The $[2Fe]_H$ subcluster, which is the site of substrate binding, is characterized by the presence of biologically unusual ligands, i.e., carbonyls, cyanides, as well as a dithiomethylamine residue (DTN), whose amine group is thought to behave as a proton shuttle during catalysis.

The structure of the $[2Fe]_H$ subcluster has inspired hundreds of biomimetic studies to date.[1] However, the catalytic efficiency of synthetic diiron catalysts always turned out to be much lower than that of the enzyme. In fact, the enzymatic Fe−S cofactor has unique stereoelectronic characteristics that are extremely difficult to reproduce in synthetic complexes.[2−4] As an example, electronic communication between the two components of the H-cluster is facile,[2,5,6] allowing electrons to easily flow from the $[Fe_4-S_4]_H$ subcluster to the $[2Fe]_H$ site.[7] In particular, the H-cluster can be reduced at mild potentials and undergo subsequent intramolecular electron transfer events functional for catalysis as a result of proton binding to the $[2Fe]_H$ site.[7] Such a key property of the [FeFe]-hydrogenases active site can be modeled in a synthetic binuclear model only if the coordination sphere of the iron atoms is designed to include a suitable noninnocent ligand that is able to behave as a surrogate of the $[Fe_4-S_4]_H$ subcluster. Very recently, steps forward in this direction have been made with the synthesis and characterization[8] of a diiron compound (**1**, see Scheme 2) including the 2,3-bis(diphenylphosphino)maleic anhydride (bma).[9] With respect to typical phosphine ligands previously used in biomimetic complexes,[1,10] the novelty of bma resides in the availability of a low-lying $\pi^*$ orbital delocalized on the maleic anhydride ring, ready to accept reducing equivalent(s) at relatively mild potentials. Actually, complex **1** (see Scheme 2) undergoes monoelectron reduction—leading to $[\mathbf{1}]^-$—at a potential at least 0.75 eV less negative than those of previous biomimetic complexes, thus suggesting that the bma ligand is the actual electron recipient in the redox event.[8] However, it was shown that reduction of the bma ligand facilitates neither electron transfer to the bimetallic portion nor protonation of the metal centers by acids,[8] the latter being a crucial event preceding $H_2$ electrocatalytic formation on biomimetic complexes.[1,11,12] Protonation of the reduced bma moiety in $[\mathbf{1}]^-$ is favored instead,[8] an event that is not functional for the catalysis of protons reduction.

In the present contribution, we report a theoretical characterization of complex $[\mathbf{1}]^-$ and of its iron-protonated counterpart. Computational data give support to the experimental findings

**Received:** February 11, 2011
**Published:** July 05, 2011

  

**Scheme 1. Structure of the H-Cluster**

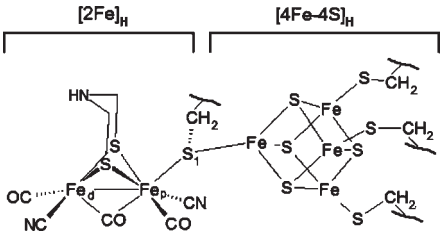


**Scheme 2. Schematic Structure of the Bma-Containing Complex**

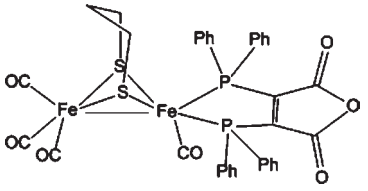


indicating that $1e^-$ reduction takes place at the bma ligand in $[\mathbf{1}]^-$ and show that electron transfer between the reduced bma ligand and the diiron portion of the complex would not take place even if the diiron moiety were protonated. Targeted modifications of the phosphine ligand are then explored, aiming at improving the properties of synthetic complexes in a biomimetic perspective. A comparison is then made between the biomimetic models and the corresponding states of the enzyme active site, in order to compare protonation regiochemistry, and therefore novel approaches for a better reproduction of the H-cluster redox chemistry in synthetic clusters are proposed.

## METHODS

All geometry optimizations were carried out using approaches already employed in our laboratories to study transition-metal complexes[13] (BP86-RI/TZVP level[14] using the Turbomole[15] program suite). Redox potentials were also computed as previously described.[12] In the case of biomimetic dinuclear and trinuclear model complexes, reaction energies are based on the total energies computed for the various complexes optimized in a vacuum at the above-reported level of theory.[16] For the computation of Mulliken charges and spin populations, we performed also single point B3LYP[17] SCF calculations at the BP86 geometries. This choice stems from the fact that BP86 is known to give extremely good performance in terms of reproduction of the structural features of H-clusters models.[4,11b] However, when it comes to electron and spin density transfers computation, BP86 is known to overestimate delocalization phenomena,[18] and thus, we rely on B3LYP charges and spin populations for the present investigation. Notice, however, that the conclusions of the present work are essentially unaffected by the choice of the functional (BP86 charges and spin populations not shown).

The procedures above-reported were applied also for $Fe_6S_6$ models of the H-cluster, with the only difference being that geometry optimizations were carried out using the COSMO solvation model[19] at $\varepsilon = 4$.[20] In fact, given the relatively large negative charge of hexanuclear model complexes (up to −5), vacuum minimizations gave place to structural instability in some of the assemblies. However, the use of the continuum solvent model to represent the stabilizing effects of the protein matrix on the clusters proved ideal for a reliable modeling in this case. Finally, the antiferromagnetic coupling in the $Fe_4S_4$ subcluster of the hexanuclear complexes has been modeled using the broken symmetry (BS) approach[21] and a recently developed approach for fast generation of BS states[22] (the BS coupling scheme used for all $Fe_6S_6$ models here discussed is shown in the Supporting Information).

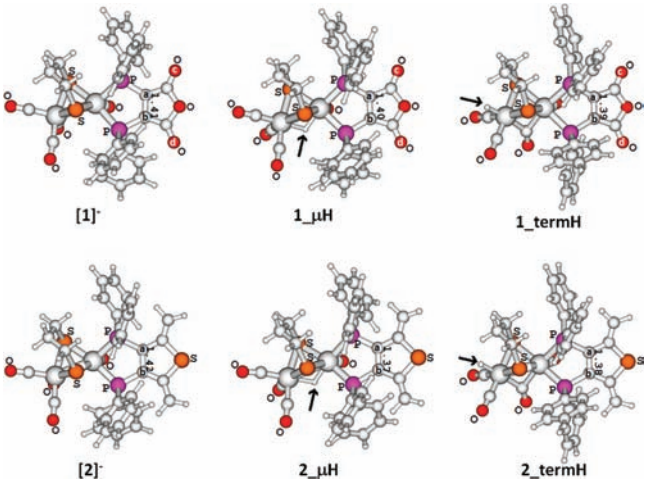


**Figure 1.** Optimized geometries of models $[\mathbf{1}]^-$, **1_μH**, **1_termH**, $[\mathbf{2}]^-$, **2_μH**, and **2_termH**. All interatomic distances are in Å. Iron, carbon, and hydrogen atoms are represented with white spheres of large, medium, or small size, respectively. Oxygen, sulfur, and phosphorus atoms are colored in red, yellow, violet, respectively, whereas the hydride ligand in models **1_μH**, **2_μH**, **1_termH**, and **2_termH** is indicated by an arrow. $C_a$, $C_b$, $O_c$, and $O_d$ atoms (see main text) have been highlighted using lower-case labels.

## RESULTS AND DISCUSSION

Before starting the discussion of our results, let us illustrate the details of the nomenclature used throughout the present paper. Biomimetic dinuclear and trinuclear complexes are named using progressive numbers: in particular, we distinguish among models of type **1** (featuring a bma ligand), **2** (featuring a diphosphine derivative of 2,5-dimethylene-2,5-dihydrothiophene), or **3** (that include a phosphine derivative of cobaltocene). Hexanuclear model complexes are also investigated and given the **sred** name, as they correspond to various possible protonation states of the super-reduced [FeFe]-hydrogenases active site (vide infra). Diphosphine derivatives of the super-reduced H-cluster are also discussed and referred to as **sred(2P)**. When applicable, specification of protonation regiochemistry is included in model names. For cationic or anionic models, the overall charge of the complexes is also explicitly specified.

**Electronic Properties of the Bma-Containing Models and Design of an Improved Noninnocent Ligand.** The first part of the present paper is devoted to the DFT characterization of the reactivity of the recently synthesized bma-containing complex **1** (Scheme 2).[8] The optimized structure of the species obtained by monoelectron reduction of **1** ($[\mathbf{1}]^-$) is reported in Figure 1, and its schematic representation is reported in Scheme 3. With respect to its neutral counterpart, $[\mathbf{1}]^-$ presents a 0.06 Å elongation of the bond between the two $sp^2$ carbon atoms belonging to the maleic anhydride ring ($C_a$ and $C_b$ in Figure 1, interatomic distance 1.41 Å). Notably, a 0.06 Å lengthening of the corresponding C−C bond in metal-bound bis(diphenylphosphino)maleic *N*-methylimide upon one-electron reduction of the maleic ring was reported also by Bensmann and Fenske, based on crystallographic investigation of mononuclear

**Scheme 3. Sketches of Models of $[1]^-$, 1_termH, and 1_$\mu$H[a]**

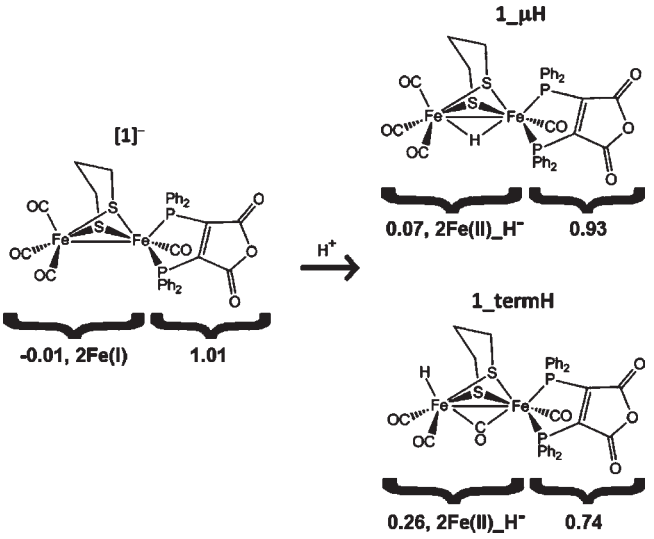


[a] For each model, spin populations of the iron-containing core (i.e., the portion of the clusters that includes Fe atoms, all carbonyl ligands, and the propanedithiolate residue bridging the two iron centers, as well as the hydride ligand in the case of **1_$\mu$H**, and **1_termH**) and of the 2,3-bis(diphenylphosphino)maleic anhydride ligand (bma) are reported under the curly brackets. Formal redox states of the iron atoms have been assigned on the basis of spin population values, as well as on the differences in Mulliken charges discussed in the main text (notice that hydride ligands have always been assigned a −1 formal charge).

**Table 1. Computed and Experimental Redox Potential Values (vs $Fc^+/Fc$, in V) for Selected Redox Couples**

| redox couple | computed redox potential | experimental redox potential |
|---|---|---|
| $1/[1]^-$ | −0.7 | −0.9 |
| $1\_HC_a/[1\_HC_a]^-$ | −0.3 | > −0.9[a] |
| $1\_\mu H/[1\_\mu H]^-$ | −1.4 | – |

[a] Lower-bound value assigned, on the basis of experimental data, to the $1\_HC_a/[1\_HC_a]^-$ (see ref 8).

Fe and Pd complexes.[9h] As far as reduction of model **1** is concerned, spin populations of $C_a$ and $C_b$ in $[1]^-$ are as large as 0.29 and 0.32, respectively. This, together with the spin population values of oxygen atoms in the bma ligand (0.15 for both $O_c$ and $O_d$, see Figure 1), confirms that the $\pi^*$ orbital delocalized over the ring is the recipient of the reducing equivalent in the $1 + e^- \rightarrow [1]^-$ reduction.[8] Consistently, the spin population is zero for both iron atoms in $[1]^-$ and, more generally, the sum of the spin population values for atoms not belonging to the bma ligand is zero as well (Scheme 3). Moreover, the sum of the Mulliken charges for the same atoms becomes only 0.19 *e* more negative as a result of $1 + e^- \rightarrow [1]^-$ reduction; in other words, the iron and sulfur atoms of the complex behave as spectators in the latter reduction reaction, further supporting the conclusions based on previous electrochemical results.[8] Finally, the computed redox potential for the $1/[1]^-$ couple is −0.7 V vs $Fc^+/Fc$ (see Table 1), a value that compares reasonably well with the experimental data (−0.9 V).[8]

**Table 2. Mulliken Charges of the Organophosphine Ligand and of the Iron-Containing Portion of Models 1, $[1]^-$, 1_$\mu$H, 1_termH and 2, $[2]^-$, 2_$\mu$H, 2_termH**

| | Mulliken Charge | |
|---|---|---|
| model | phosphine ligand | Fe-harboring portion[a] |
| **1** | 0.40 | −0.40 |
| $[1]^-$ | −0.41 | −0.59 |
| **1_$\mu$H** | −0.05 | 0.05 |
| **1_termH** | 0.12 | −0.12 |
| **2** | 0.38 | −0.38 |
| $[2]^-$ | −0.36 | −0.64 |
| **2_$\mu$H** | 0.37 | −0.37 |
| **2_termH** | 0.40 | −0.40 |

[a] This portion includes the Fe atoms, all the carbonyl ligands, and the propanedithiolate residue bridging the two iron centers, as well as the hydride ligand in **1_$\mu$H**, **1_termH**, **2_$\mu$H**, and **2_termH**.

In order to evaluate the feasibility of electron transfer between the bma ligand and the rest of the complex, we initially optimized model **1_$\mu$H** (Scheme 3 and Figure 1), i.e., a hypothetical $\mu$-H adduct originating from protonation of $[1]^-$. Such a model has been investigated keeping in mind that, in [FeFe]-hydrogenases, protonation of the $[2Fe]_H$ subsite can trigger electron transfer events, thus tightly coupling the two fundamental events in proton reduction catalysis. However, electron transfer from the reduced bma ligand to the diiron moiety is not observed on going from $[1]^-$ to **1_$\mu$H**. In fact, the latter features a spin population value on the bma ligand as large as 0.93 (see Scheme 3). As a consequence, the remaining portion of the **1_$\mu$H** model, which includes the $\mu$-H bound Fe atoms, features a low spin population value (0.07). This result shows that the electron residing in the $\pi^*$ orbital of the maleic anhydride ring is stable, thanks to the presence of three highly electronegative oxygen atoms in the bma ligand that favor delocalization by means of resonance effects. In this context, it is worth noting that the $C_a-C_b$ distance in **1_$\mu$H** is 1.40 Å, essentially identical to the 1.41 Å length found for the same bond in $[1]^-$ (see Figure 1). As far as charge transfer is concerned, protonation of metal centers leads to a rather small electron density withdrawal from the bma ligand toward the metal-containing portion of the complex; in fact, the bma moiety becomes only 0.36 *e* less negatively charged, following the $[1]^- + H^+ \rightarrow$ **1_$\mu$H** protonation (see Table 2).

Terminal hydride adducts are expected to be more reactive than their $\mu$-H counterparts, as far as $H_2$ evolution is taken into account.[23] Therefore, we characterized also the model **1_termH** (Scheme 3 and Figure 1). Such an adduct is significantly higher in energy then the bridging-hydride isomer ($\Delta E_{1\_termH-1\_\mu H}$ = 9.9 kcal/mol). However, it is noteworthy that the formation of a terminal hydride following the $[1]^- + H^+ \rightarrow$ **1_termH** protonation mechanism would lead to a withdrawal of electron density from the bma ligand that is more pronounced than in the $[1]^- + H^+ \rightarrow$ **1_$\mu$H** reaction. In fact, the charge of the bma moiety is +0.12 in **1_termH**, a value 0.53 *e* charge units larger than in $[1]^-$ (see Table 2). Consistently, the Fe-harboring portion of **1_termH** acquires a spin population that, though small, is significant, 0.26 (Scheme 3). Notably, the main contribution is given by the iron atom not bound to the hydride, the spin population of which is 0.27 (spin population of the hydride-bound Fe atom, 0.04). However, the $C_a$ and $C_b$ spin populations (0.25 and


dx.doi.org/10.1021/ic200297d |*Inorg. Chem.* 2011, 50, 6987–6995

**Scheme 4. Comparison between the Bma Ligand (on the left) and the Bis(diphenylphosphino) Derivative of 2,5-Dimethylene-2,5-dihydrothiophene (on the right)**

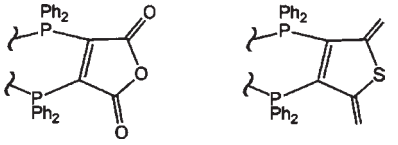

0.26, respectively) are only slightly smaller than those of the same atoms in $[\mathbf{1}]^-$ (0.29 and 0.32; see above), a fact that witnesses substantial occupation of the $\pi^*$ orbital of the maleic anhydride ring also in **1_termH**.

The above results indicate that the bma ligand and the diiron tetracarbonyl core form a poorly matched couple, as far as the reproduction of proton-induced electron transfers in [FeFe]-hydrogenases is concerned. In order to better balance the redox properties of the diiron core and of the phosphine ligand, we focused on possible strategies to tune the reduction potential of the latter. In fact, it has to be noted that the free bma ligand shows a reversible reduction process at −1.1 V in MeCN,[8] while the redox potential of biomimetic diphosphine diiron complexes typically resides in a range between −2.0 and −2.4 V.[24] The poor match between the maleic ring and the iron-harboring portion of **1** indicates that the gap between their redox potentials is too large to allow the coupling of proton and electron transfers.[25] In view of the above considerations, we tested the effects of the substitution of the two carbonyl oxygen atoms in the bma ligand with methylene groups and of the contextual substitution of the anhydridic oxygen atom in the ring with a less electronegative sulfur atom (see Scheme 4 and models $[\mathbf{2}]^-$ and **2_μH** in Figure 1 and Scheme 5; the phosphine ligand in these complexes is a derivative of the 2,5-dimethylene-2,5-dihydrothiophene (dmdh) molecule previously described in the literature[26]).

Model $[\mathbf{2}]^-$ features a unitary spin population value on the phosphine ligand. Consequently, the iron atoms and the remaining portions of the metals coordination sphere have overall zero spin population (Scheme 5). Moreover, the latter region of the complex is only slightly more negatively charged in $[\mathbf{2}]^-$ than in the neutral, unprotonated parent complex (model **2**, structure not shown; see Table 2). As far as the $C_a-C_b$ bond in $[\mathbf{2}]^-$ is taken into account, its length (1.42 Å, see Figure 1) is very similar to the corresponding one in $\mathbf{1}^-$, an observation that again witnesses a partial filling of the $\pi^*$ orbital in the $[\mathbf{2}]^-$ pentatomic heterocyclic ring. However, protonation of metal centers in $[\mathbf{2}]^-$ leads to a large reorganization of the stereoelectronic properties of the complex. In fact, **2_μH** features a shortening of the $C_a-C_b$ bond length by 0.05 Å, indicating that the above-mentioned antibonding orbital is now empty. Consistently, **2_μH** shows a negligible spin population value at the dmdh ligand (Scheme 5), whereas the unpaired electron resides on the metal-containing portion of the complex (spin population 0.96, Scheme 5). Analysis of Mulliken atomic charges reveals that modification of the organophosphine ligand also leads to a significant enhancement of the charge transfer toward the iron-harboring portion of the complex as a result of protonation. In fact, the latter region of the cluster withdraws −0.73 *e* from the dmdh ligand as a result of the $[\mathbf{2}]^- + H^+ \rightarrow$ **2_μH** protonation reaction (see Table 2). Therefore, the above results show how protonation of metal centers in $[\mathbf{2}]^-$ is able to trigger the transfer of the

**Scheme 5. Sketches of Models of $[\mathbf{2}]^-$, 2_termH, and 2_μH[a]**

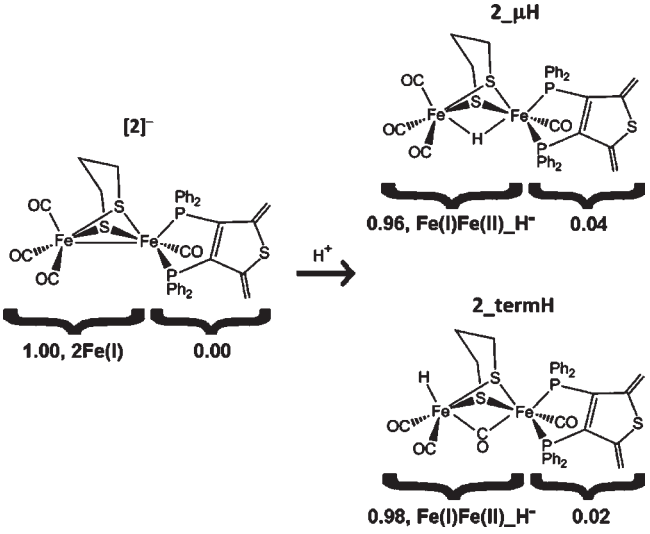


[a] For each model, spin populations of the iron-containing core (i.e., the portion of the clusters that includes Fe atoms, all carbonyl ligands, and the propanedithiolate residue bridging the two iron centers, as well as the hydride ligand in the case of **2_μH**, and **2_termH**) and of the bis-(diphenylphosphino) derivative of dmdh are reported under the curly brackets. Formal redox states of the iron atoms have been assigned on the basis of spin population values, as well as on the differences in Mulliken charges discussed in the main text (notice that hydride ligands have always been assigned a −1 formal charge).

unpaired electron from the phosphine ligand to the hydride-bound portion of the complex.

Finally, we optimized the terminal-hydride isomer **2_termH** (Scheme 5 and Figure 1), which is 7.8 kcal/mol higher in energy than the bridging-hydride counterpart and features charges and spin population values similar to the ones observed in **2_μH** (see Table 2 and Scheme 5). Thus, the $[\mathbf{2}]^- + H^+ \rightarrow$ **2_termH** protonation reaction leads to a reorganization of the electronic structure analogous to the one above-described in the case of the $\mu$-H adduct.

**Protonation Regiochemistry in the Biomimetic Models and in the Corresponding H-Cluster States.** The above results show that it is in principle possible to reproduce some key electronic features of the H-cluster $Fe_4S_4$ subcluster in biomimetic complexes, by designing organophosphine ligands that can behave as a reservoir of electrons. Another relevant issue in the design of biomimetic complexes is the protonation regiochemistry of the complex after its monoelectron reduction. As explained in the Introduction, it is experimentally found that complex $[\mathbf{1}]^-$ is protonated at the bma ligand rather than at the metal centers. Thus, reaction of $[\mathbf{1}]^-$ with Brønsted−Lowry acids does not lead to proton-induced intramolecular electron transfer toward the latter. This case is paradigmatic, as it highlights that the reproduction of naturally occurring proton-induced electron transfers in biomimetic complexes requires the introduction of noninnocent ligands that show suitable redox properties and relatively low basicity at the same time.

DFT results indicate that model **1_μH** is essentially isoenergetic with an isomer featuring protonation of the $C_a$ atom of the bma ligand (adduct $\mathbf{1\_HC_a}$, optimized geometry reported in Supporting Information, $\Delta E_{\mathbf{1\_HC_a}-\mathbf{1\_\mu H}} = 0.0$ kcal/mol). All the


dx.doi.org/10.1021/ic200297d |*Inorg. Chem.* 2011, 50, 6987–6995

Scheme 6. Sketches of Super-Reduced H-Cluster Models and of Their Bridging or Terminal Hydride Derivatives[a]

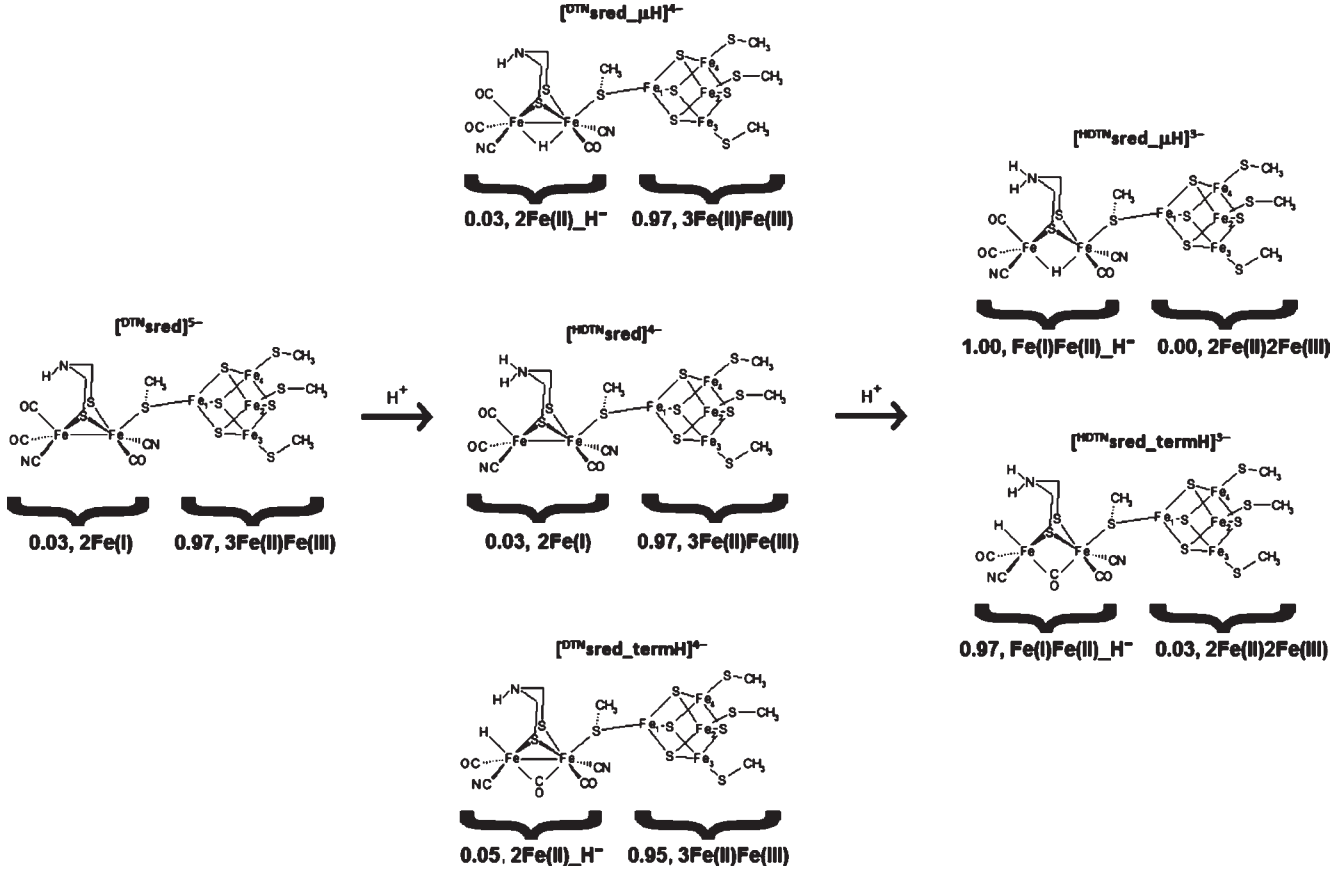


[a] For each model, spin populations of the binuclear and tetranuclear subclusters are reported under the curly brackets; notice that the bridging $CH_3S^-$ group has been completely assigned to the tetranuclear portion, as far as spin populations calculations are concerned. Formal redox states of the iron atoms have been assigned on the basis of spin population values, as well as on the differences in Mulliken charges discussed in the main text (notice that hydride ligands have always been assigned a −1 formal charge).

other possible protonation sites in bma, namely, the oxygen atoms, turned out to be significantly less basic (data not shown) and are thus considered to be irrelevant in the context of the reactivity of $[\mathbf{1}]^-$ with acids. Therefore, DFT results are compatible with the experimental findings regarding the important role of the reduced bma ligand in the interaction with protons. Moreover, the calculated redox potential of $\mathbf{1\_HC_a}$ is −0.3 V, in full agreement with experiments indicating that the bma-protonated, neutral adduct has a redox potential less negative than −0.9 V (compare the latter value also with the redox potential calculated for the $\mu$-H isomer $\mathbf{1\_\mu H}$, which is much more negative, −1.4 V; Table 1). As for the prediction of protonation regiochemistry in the dmdh-containing models, the picture is analogous to the one described for models of the **1** type. In fact, the computed energy of model $\mathbf{2\_HC_a}$ (optimized geometry in Supporting Information) is slightly lower than for the corresponding $\mu$-H isomer $\mathbf{2\_\mu H}$ ($\Delta E_{\mathbf{2\_HCa-2\_\mu H}} = -1.8$ kcal/mol). In other words, model $\mathbf{2}^-$ is likely to be not significantly different from model $\mathbf{1}^-$ in terms of reactivity toward acids, as protonation of the organophosphine ligand is predicted to be favored over formation of a $\mu$-hydride adduct.

The above results stimulated us to investigate the protonation regiochemistry of states of the H-cluster corresponding to the monoanionic, unprotonated biomimetic adducts ($[\mathbf{1}]^-$ and $[\mathbf{2}]^-$), which formally correspond to Fe(I)Fe(I) species. Interestingly, recent electrochemical,[27] spectroelectrochemical,[28] and theoretical data[29] point toward the presence of a dihypoferrous $[2Fe]_H$ subsite not only in the $H_{red}$ redox state but also in the super-reduced enzyme form ($H_{sred}$, an enzyme form typically obtained at potentials around −0.5 V). In particular, the results of these studies suggest that $H_{sred}$ features an Fe(I)Fe(I) $Fe_2S_2$ and an electron-rich 3Fe(II)Fe(III) $Fe_4S_4$ subcluster, resembling the reduced state of the organophosphine ligands in $[\mathbf{1}]^-$ and $[\mathbf{2}]^-$. Even though the relevance of $H_{sred}$ in the catalytic cycle is doubtful, the protonation of its metal centers leads to adducts that might have relevance during $H_2$ evolution/oxidation.[7] As for the structural features of the H-cluster in $H_{sred}$, computation of IR spectra led to the proposal that a mixture of two enzyme states determines the experimentally observed absorption bands.[28,29] In particular, since the formation of the super-reduced enzyme is found to be accompanied by the disappearance of the $\mu$-CO IR band,[28] both such states were proposed to present a bridging-to-terminal redisposition of the $\mu$-CO ligand,[29] while the main difference between them is the protonation state of the amine group of the DTN moiety.[29] Such two states of the $Fe_6S_6$ clusters are here considered in order to further characterize the super-reduced form of the enzyme: we optimized models $[^{\mathbf{DTN}}\mathbf{sred}]^{5-}$ and $[^{\mathbf{HDTN}}\mathbf{sred}]^{4-}$ (schematic structures reported in Scheme 6).


dx.doi.org/10.1021/ic200297d |Inorg. Chem. 2011, 50, 6987–6995

**Scheme 7. Sketches of Models $[^{HDTN}sred(2P)]^{2-}$, $[^{HDTN}sred(2P)\_\mu H]^{-}$, and $[^{HDTN}sred(2P)\_termH]^{-}$**[a]

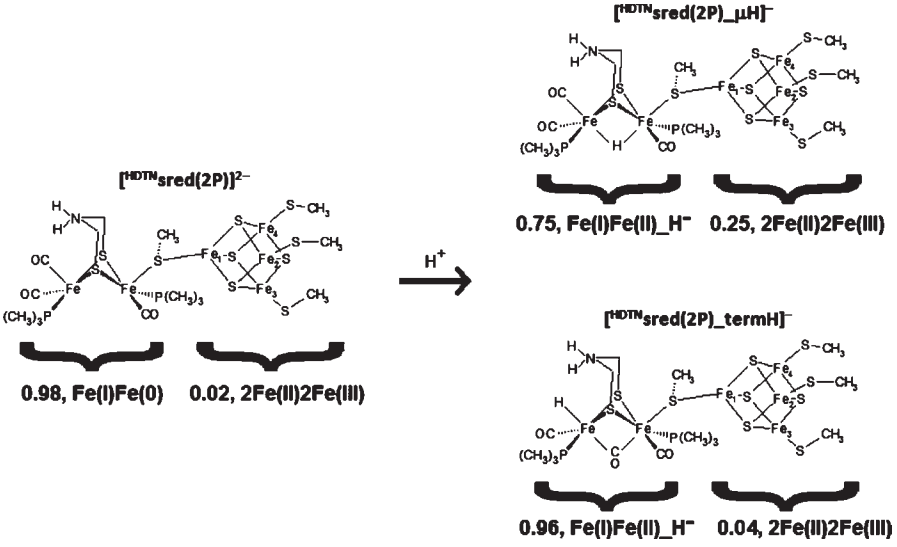


[a] For each model, spin populations and Fe atoms formal redox states have been assigned as described in the caption of Scheme 6.

Subsequent computation of spin populations gives a value close to zero for the $[2Fe]_H$ subcluster in both models, further supporting the hypothesis that the binuclear cluster in $H_{sred}$ is in the diamagnetic Fe(I)Fe(I) state.

Let us now consider the possibility of coupled proton and electron transfers in $H_{sred}$. Intramolecular transfer of an $H^+$ from the DTN residue to the iron centers of the $[2Fe]_H$ site leads to $[^{DTN}\mathbf{sred\_\mu H}]^{4-}$ (Scheme 6). Previous results indicate that there is no substantial difference between $[^{DTN}\mathbf{sred\_\mu H}]^{4-}$ and the parent complex $[^{HDTN}\mathbf{sred}]^{4-}$, in terms of localization of the unpaired electron.[7] Similar considerations hold true for the terminal-hydride isomer $[^{DTN}\mathbf{sred\_termH}]^{4-}$. For the sake of completeness, spin population values computed as described in the Methods are reported for both $[^{DTN}\mathbf{sred\_\mu H}]^{4-}$ and $[^{DTN}\mathbf{sred\_termH}]^{4-}$ in Scheme 6. Then, we considered models obtained from the addition of one proton to $[^{HDTN}\mathbf{sred}]^{4-}$, leading to either a $\mu$-H or a terminal hydride (models $[^{HDTN}\mathbf{sred\_\mu H}]^{3-}$ and $[^{HDTN}\mathbf{sred\_termH}]^{3-}$, Scheme 6). In the latter adducts the unpaired electron was found to be localized on the $[2Fe]_H$ subcluster.[7] When considering charge transfer, protonation of the $[2Fe]_H$ site leads to a pronounced electron density withdrawal from the tetranuclear portion toward the binuclear site. In fact, the $Fe_4S_4$ moiety becomes 0.81 and 0.79 *e* less negatively charged upon $[^{HDTN}\mathbf{sred}]^{4-} + H^+ \rightarrow [^{HDTN}\mathbf{sred\_\mu H}]^{3-}$ and $[^{HDTN}\mathbf{sred}]^{4-} + H^+ \rightarrow [^{HDTN}\mathbf{sred\_termH}]^{3-}$ protonations, respectively. Taken as a whole, these results show that protonation of metal centers in the $H_{sred}$ model $[^{HDTN}\mathbf{sred}]^{4-}$ leads to the transfer of an unpaired electron from the tetranuclear portion of the cluster toward the $[2Fe]_H$ subsite.

Notably, the above picture is fully superimposable with the reorganization of the electron density computed in the $[\mathbf{2}]^- + H^+ \rightarrow \mathbf{2\_\mu H}$ protonation reaction described above, in Table 2 and Scheme 5. However, relevant differences between the H-cluster and biomimetic analogues can be noticed when protonation regiochemistry is taken into account. In fact, $[^{HDTN}\mathbf{sred}]^{4-}$ is at least 11 kcal/mol lower in energy than any of the possible isomers resulting from single protonation of basic sulfur centers in the $Fe_4S_4(SCH_3)_3$ moiety (optimized geometries not shown). In other words, when the naturally occurring coordination of the iron ions is preserved in the $[Fe_4S_4]_H$ cubane (i.e., each Fe atoms is bound to three inorganic sulfides and a cysteine sulfur atom), its basicity is relatively low, even in the case of the reduced, 3Fe(II)Fe(III) state.

The last step of our investigation of hexanuclear clusters consists of optimizations of modified versions of the H-cluster, in which cyanides are substituted with $P(CH_3)_3$ groups (species $[^{HDTN}\mathbf{sred(2P)}]^{2-}$, $[^{HDTN}\mathbf{sred(2P)\_termH}]^{-}$, and $[^{HDTN}\mathbf{sred(2P)\_\mu H}]^{-}$; see Scheme 7). Such calculations are relevant from the perspective of designing novel synthetic $Fe_6S_6$ model compounds, since cyanides can compete with metal centers for protons binding. However, calculated spin populations show that the unpaired electron resides on the binuclear subsite not only in the hydride complexes $[^{HDTN}\mathbf{sred(2P)\_termH}]^{-}$ and $[^{HDTN}\mathbf{sred(2P)\_\mu H}]^{-}$ but also in the parent complex with unprotonated metal centers $[^{HDTN}\mathbf{sred(2P)}]^{2-}$ (Scheme 7). Consistently, protonation of the diiron site leads to a small electron density withdrawal from the tetranuclear portion of the cluster. In fact, the $Fe_4S_4$ moiety becomes 0.27 and 0.13 *e* less negatively charged as a result of $[^{HDTN}\mathbf{sred(2P)}]^{2-} + H^+ \rightarrow [^{HDTN}\mathbf{sred(2P)\_\mu H}]^{-}$ and $[^{HDTN}\mathbf{sred(2P)}]^{2-} + H^+ \rightarrow [^{HDTN}\mathbf{sred(2P)\_termH}]^{-}$ protonation reactions, respectively. This indicates that the diphosphine hexanuclear model fails to reproduce the properties of the corresponding dicyanide species, in terms of proton-induced electron transfer events.

**Complexes Including a Phosphine Derivative of Cobaltocene Well-Reproduce the Electron-Transfer Events Observed in the H-Cluster.** Recent advances in biomimetic modeling of the H-cluster allowed introduction of ferrocene derivatives in the iron coordination sphere.[30] This approach is promising, as far as reproduction of [FeFe]-hydrogenases redox chemistry is concerned. In fact, metallocenes are widely available redox-active species, the redox potential of which can be tuned by varying the nature of the coordinating metal and the substituents bound to the cyclopentadienyl rings. For example, taking ferrocene as a reference, the redox potential of the cobaltocenium/cobaltocene couple results to be as negative as −1.33 V. In other


dx.doi.org/10.1021/ic200297d |*Inorg. Chem.* 2011, 50, 6987–6995

**Scheme 8. Sketches of Models of type 3**[a]

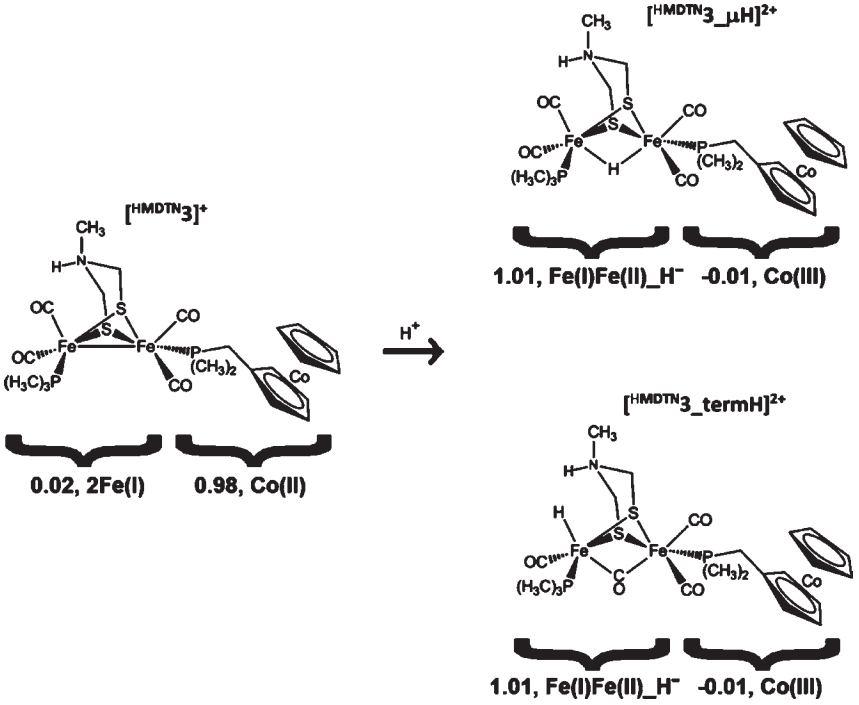


[a] In correspondence of the curly brackets, spin populations for the binuclear and mononuclear portions of the models are reported [the bridging $(CH_3)_2P$ fragment has been completely assigned to the metallocene portion]. Formal redox states of metal atoms have been attributed as described in the caption of Scheme 6.

words, replacing Fe with Co allows one to widely shift the metallocenium/metallocene couple toward the redox potential range typical of biomimetic phosphine-substituted diiron complexes.[24] Prompted by these observations and by DFT results for the super-reduced H-cluster, we studied the electronic properties of a diphosphine complex featuring an amine group in the pendant and a cobaltocene derivative attached to one of the phosphorus atoms. Our efforts to couple proton and electron transfers in analogy with the super-reduced H-cluster model led us to investigate model $[^{HMDTN}\mathbf{3}]^+$ and its derivatives ($[^{HMDTN}\mathbf{3\_\mu H}]^{2+}$ and $[^{HMDTN}\mathbf{3\_termH}]^{2+}$; see Scheme 8). They all feature a protonated tertiary amine (a methyldithiomethylamine residue indicated as MDTN in the model names, or HMDTN in case of amine group protonation). Moreover, the doubly protonated model $[^{HMDTN}\mathbf{3\_\mu H}]^{2+}$ features also a metal-bound $\mu$-$H^-$ group similarly to complexes recently synthesized by Ott and co-workers.[31] Model $[^{HMDTN}\mathbf{3\_termH}]^{2+}$ is a terminal-hydrido isomer instead.

In $[^{HMDTN}\mathbf{3}]^+$, the unpaired electron is localized at the level of its cobalt-containing portion (Mulliken spin population value 0.98, indicating a Co(II) ion). However, after protonation of the diiron moiety (model $[^{HMDTN}\mathbf{3\_\mu H}]^{2+}$; Scheme 8), the unpaired electron moves toward the diiron portion of the model (Mulliken spin population of the diiron moiety in $[^{HMDTN}\mathbf{3\_\mu H}]^{2+}$, 1.01; see Scheme 8). The one-electron oxidation of the Co-containing portion of the model is also illustrated by the variation of its Mulliken charge value, which goes from 0.47 in $[^{HMDTN}\mathbf{3}]^+$ to 1.32 in $[^{HMDTN}\mathbf{3\_\mu H}]^{2+}$. Very similar considerations hold true in the case of $[^{HMDTN}\mathbf{3}]^+ + H^+ \rightarrow [^{HMDTN}\mathbf{3\_termH}]^{2+}$ protonation (computed charge of the Co-containing portion in the latter model, 1.29).

Notice that, analogously to the case of the super-reduced H-cluster, an intramolecular proton transfer from the methyldithiomethylamine ligand to the iron atoms is not sufficient to trigger electron transfer toward the diiron subsite. This conclusion is based on computation of the spin population of the diiron subsite in model complexes featuring a deprotonated amine in the pendant and a Fe-bound hydride, the latter either in terminal or bridging position (models $[^{MDTN}\mathbf{3\_termH}]^+$ and $[^{MDTN}\mathbf{3\_\mu H}]^+$, respectively; both models have spin populations at the diiron subsite close to zero, analogously to the parent model $[^{HMDTN}\mathbf{3}]^+$; see also Supporting Information).

## CONCLUSIONS

Recent advances in the modeling of [FeFe]-hydrogenases chemistry in synthetic binuclear clusters have allowed the synthesis of $[Fe_2(\mu\text{-}S_2(CH_2)_3)(CO)_4(bma)]$ (**1**), which features a noninnocent organophosphine ligand (bma) that can undergo monoelectron reduction, analogously to the tetranuclear $Fe_4S_4$ subcluster in the H-cluster.[8] This research line is crucial for the development of biomimetic complexes able to reproduce the intramolecular redox chemistry operative in the active site of [FeFe]-hydrogenases.

Previous experimental results indicated that monoelectron reduction of complex **1** is localized at the bma moiety. However, when it comes to reactivity toward protic acids, the reduced anhydridic ring of bma proved sufficiently basic to compete with the catalytically active iron centers, thus impairing electrocatalytic $H_2$ evolution. DFT results are consistent with experimental findings, since computation of Mulliken charges and spin populations shows that the iron-containing portion of the cluster remains a spectator in the redox process $\mathbf{1} + e^- \rightarrow [\mathbf{1}]^-$. Moreover,


dx.doi.org/10.1021/ic200297d |*Inorg. Chem.* 2011, 50, 6987–6995

we have shown that even if proton binding could take place at the metal centers, it would not trigger transfer of the unpaired electron from the bma ligand to the iron-containing portion of the model. However, partial charge transfer is detected in the terminal hydride complex **1_termH**, even though the latter is higher in energy than the bridging hydride isomer **1 $\mu$H**.

By means of targeted modifications of the noninnocent ligand, it is possible to establish electronic communication between the two portions of the cluster, such that the coupling between proton and electron transfers toward the metal centers is restored, and intramolecular charge transfer events are enhanced as well. In fact, models designed to contain a phosphine derivative of 2,5-dimethylene-2,5-dihydrothiophene show a tight coupling between proton and electron transfers upon $[\mathbf{2}]^- + H^+ \rightarrow \mathbf{2\_\mu H}$ protonation reaction, a fact that has no counterpart in the $[\mathbf{1}]^- + H^+ \rightarrow \mathbf{1\_\mu H}$ protonation.

However, both in the bma-containing ligand and in the 2,5-dimethylene-2,5-dihydrothiophene derivative, protonation of the organic ligand is favored over protonation of the iron centers in the complexes. Conversely, protonation of the corresponding iron ions in models of the isolated [FeFe]-hydrogenases active site is largely favored, as compared to proton attachment to the tetranuclear unit of the H-cluster. Our efforts to individuate electron-donating moieties with suitable redox properties and lower affinity toward protons led us to investigate trinuclear complexes in which the diiron pentacarbonyl fragment is linked to a cobaltocene residue by means of a $P(CH_3)_2CH_2$ bridge. It turned out that a facile electron transfer event similar to the one occurring in the super-reduced form of the H-cluster takes place upon protonation of the iron atoms of the trinuclear model complex (reactions $[^{HMDTN}\mathbf{3}]^+ + H^+ \rightarrow [^{HMDTN}\mathbf{3\_\mu H}]^{2+}$ and $[^{HMDTN}\mathbf{3}]^+ + H^+ \rightarrow [^{HMDTN}\mathbf{3\_termH}]^{2+}$). Even if cobaltocene slowly degrades when exposed to acids[32] and $[^{HMDTN}\mathbf{3}]^+$ is likely to require strong acids to be protonated at the metals,[31] it is tempting to propose that proton-induced electron transfers in complexes of this kind might be detected, at least transiently, in targeted spectroelectrochemical experiments. In this regard, it is crucial to understand that the reproduction of naturally occurring proton-induced electron transfers in biomimetic complexes requires the introduction of noninnocent ligands that show suitable redox properties and relatively low basicity at the same time. Notably, protonation of iron centers following $[^{HMDTN}\mathbf{3}]^+ + H^+ \rightarrow [^{HMDTN}\mathbf{3\_\mu H}]^{2+}$ results to be ~9 kcal/mol favored with respect to cobaltocene protonation (reactions $[^{HMDTN}\mathbf{3}]^+ + H^+ \rightarrow [^{HMDTN}\mathbf{3\_HCp_1}]^{2+}$ and $[^{HMDTN}\mathbf{3}]^+ + H^+ \rightarrow [^{HMDTN}\mathbf{3\_HCp_2}]^{2+}$; see Supporting Information for structural schemes and mechanistic details).

## ■ ASSOCIATED CONTENT

**Supporting Information.** Optimized structures and schematic representations of models **1_HC$_a$**, **2_HC$_a$**, $[^{MDTN}\mathbf{3\_termH}]^+$, $[^{MDTN}\mathbf{3\_\mu H}]^+$, $[\mathbf{1(CN)_2}]^{3-}$, $[\mathbf{1(CN)_2termH}]^{2-}$, $[\mathbf{1(CN)_2\_\mu H}]^{2-}$, $[^{HMDTN}\mathbf{3\_HCp_1}]^{2+}$, and $[^{HMDTN}\mathbf{3\_HCp_2}]^{2+}$; BS coupling scheme used for hexanuclear model complexes. This material is available free of charge via the Internet at http://pubs.acs.org.

## ■ AUTHOR INFORMATION

### Corresponding Author

*E-mail: claudio.greco@unimib.it. Fax: +390264483478.

## ■ ACKNOWLEDGMENT

The authors would like to thank the anonymous reviewers for their valuable comments and precious suggestions. CINECA (Bologna, Italy) is also gratefully acknowledged for having provided high-performance computational resources.

## ■ REFERENCES

(1) Tard, C.; Pickett, C. J. *Chem. Rev.* **2009**, *109*, 2245–2274.

(2) Lubitz, W.; Reijerse, E.; van Gastel, M. *Chem. Rev.* **2007**, *107*, 4331–4365.

(3) Siegbahn., P. E. M.; Tye, J. W.; Hall, M. B. *Chem. Rev.* **2007**, *107*, 4414–4435. De Lacey, A. L.; Fernandez, V. M.; Rousset, M.; Cammack, R. *Chem. Rev.* **2007**, *107*, 4304–4330. Vincent, K. A.; Parkin, A.; Armstrong, F. A. *Chem. Rev.* **2007**, *107*, 4366–4413. Fontecilla-Camps, J. C.; Volbeda, A.; Cavazza, C.; Nicolet, Y. *Chem. Rev.* **2007**, *107*, 4273–4303. Peters, J. W.; Lanzilotta, W. N.; Lemon, B. J.; Seefeldt, L. C. *Science* **1998**, *282*, 1853–1858.

(4) Bruschi, M.; Zampella, G.; Fantucci, P.; De Gioia, L. *Coord. Chem. Rev.* **2005**, *249*, 1620–1640.

(5) Schwab, D. E.; Tard, C.; Brecht, E.; Peters, J. W.; Pickett, C. J.; Szilagyi, R. K. *Chem. Commun.* **2006**, 3696–3698. Silakov, A.; Reijerse, E. J.; Albracht, S. P. J.; Hatchikian, E. C.; Lubitz, W. *J. Am. Chem. Soc.* **2007**, *129*, 11447–11458.

(6) Bruschi, M.; Greco, C.; Zampella, G.; Ryde, U.; Pickett, C. J.; De Gioia, L. *C. R. Chim.* **2008**, *11*, 834–841.

(7) Bruschi, M.; Greco, C.; Kaukonen, M.; Fantucci, P.; Ryde, U.; De Gioia, L. *Angew. Chem., Intl. Ed.* **2009**, *48*, 3503–3506.

(8) Si, Y. T.; Charreteur, K.; Capon, J. F.; Gloaguen, F.; Petillon, F. Y.; Schollhammer, P.; Talarmin, J. *J. Inorg. Biochem.* **2010**, *104*, 1038–1042.

(9) (a) Bott, S. G.; Yang, K. Y.; Richmond, M. G. *J. Organomet. Chem.* **2006**, *691*, 3771–3781. (b) Yang, K. Y.; Smith, J. M.; Bott, S. G.; Richmond, M. G. *Organometallics* **1993**, *12*, 4779–4787. (c) Yang, K. Y.; Bott, S. G.; Richmond, M. G. *Organometallics* **1995**, *14*, 2387–2394. (d) Yang, K. Y.; Bott, S. G.; Richmond, M. G. *J. Organomet. Chem.* **1996**, *516*, 65–80. (e) Kandala, S.; Hammons, C.; Watson, W. H.; Wang, X. P.; Richmond, M. G. *Dalton Trans.* **2010**, *39*, 1620–1629. (f) Mao, F.; Tyler, D. R.; Keszler, D. *J. Am. Chem. Soc.* **1989**, *111*, 130–134. (g) Tyler, D. R. *Acc. Chem. Res.* **1991**, *24*, 325–331. (h) Bensmann, W.; Fenske, D. *Angew. Chem., Int. Ed. Engl.* **1979**, *18*, 677–678.

(10) Thomas, C. M.; Liu, T. B.; Hall, M. B.; Darensbourg, M. Y. *Inorg. Chem.* **2008**, *47*, 7009–7024. Wang, N.; Wang, M.; Zhang, T. T.; Li, P.; Liu, J. H.; Sun, L. C. *Chem. Commun.* **2008**, 5800–5802. Ezzaher, S.; Capon, J. F.; Dumontet, N.; Gloaguen, F.; Petillon, F. Y.; Schollhammer, P.; Talarmin, J. *J. Electroanal. Chem.* **2009**, *626*, 161–170. Chen, Z. J.; Lemon, B. J.; Huang, S.; Swartz, D. J.; Peters, J. W.; Bagley, K. A. *Biochemistry* **2002**, *41*, 2036–2043. Olsen, M. T.; Rauchfuss, T. B.; Wilson, S. R. *J. Am. Chem. Soc.* **2010**, *132*, 17733–17740. Cheah, M. H.; Borg, S. J.; Best, S. P. *Inorg. Chem.* **2007**, *46*, 1741–1750.

(11) (a) Borg, S. J.; Behrsing, T.; Best, S. P.; Razavet, M.; Liu, X. M.; Pickett, C. J. *J. Am. Chem. Soc.* **2004**, *126*, 16988–16999. (b) Greco, C.; Zampella, G.; Bertini, L.; Bruschi, M.; Fantucci, P.; De Gioia, L. *Inorg. Chem.* **2007**, *46*, 108–116.

(12) Greco, C.; Fantucci, P.; De Gioia, L.; Suarez-Bertoa, R.; Bruschi, M.; Talarmin, J.; Schollhammer, P. *Dalton Trans.* **2010**, *39*, 7320–7329.

(13) Greco, C.; Bruschi, M.; Fantucci, P.; De Gioia, L. *Eur. J. Inorg. Chem.* **2007**, 1835–1843. Schneider, C. J.; Zampella, G.; Greco, C.; Pecoraro, V. L.; De Gioia, L. *Eur. J. Inorg. Chem.* **2007**, 515–523.

(14) Becke, A. D. *Phys. Rev. A* **1988**, *38*, 3098–3100. Perdew, J. P. *Phys. Rev. B* **1986**, *33*, 8822–8824. Schafer, A.; Huber, C.; Ahlrichs, R. *J. Chem. Phys.* **1994**, *100*, 5829–5835. Eichkorn, K.; Treutler, O.; Ohm, H.; Haser, M.; Ahlrichs, R. *Chem. Phys. Lett.* **1995**, *240*, 283–289. Eichkorn, K.; Weigend, F.; Treutler, O.; Ahlrichs, R. *Theor. Chem. Acc.* **1997**, *97*, 119–124.

(15) Ahlrichs, R.; Bar, M.; Haser, M.; Horn, H.; Kolmel, C. *Chem. Phys. Lett.* **1989**, *162*, 165–169.

(16) The choice of vacuum calculations stems from the observation that results did not significantly vary after soaking bma-containing complexes in a COSMO representation of toluene ($\varepsilon$ = 2.4), a solvent used for synthesis and characterization of **1** and its derivatives. In fact, spin population and Mulliken charges of complex $[\mathbf{1}]^-$ and its terminal-hydride and bridging-hydride derivatives (see Results and Discussion) vary by less than 0.13 and 0.06 when computed in a vacuum or in a continuum solvent model at $\varepsilon$ = 2.4; moreover, the computed stability difference between the two hydride adducts vary by only 0.2 kcal/mol going from vacuum to COSMO-soaked models.

(17) Becke, A. D. *J. Chem. Phys.* **1993**, *98*, 5648–5652. Lee, C. T.; Yang, W. T.; Parr, R. G. *Phys. Rev. B* **1988**, *37*, 785–789.

(18) Matito, E.; Sola, M. *Coord. Chem. Rev.* **2009**, *253*, 647–665.

(19) Klamt, A. *J. Phys. Chem.* **1995**, *99*, 2224–2235.

(20) Gilson, M. K.; Honig, B. H. *Biopolymers* **1986**, *25*, 2097–2119.

(21) Noodleman, L.; Norman, J. G. *J. Chem. Phys.* **1979**, *70*, 4903–4906. Noodleman, L. *J. Chem. Phys.* **1981**, *74*, 5737–5743. Fiedler, A. T.; Brunold, T. C. *Inorg. Chem.* **2005**, *44*, 9322–9334.

(22) Greco, C.; Fantucci, P.; Ryde, U.; De Gioia, L. *Int. J. Quantum Chem.* In press. DOI: 10.1002/qua.22849.

(23) van der Vlugt, J. I.; Rauchfuss, T. B.; Whaley, C. M.; Wilson, S. R. *J. Am. Chem. Soc.* **2005**, *127*, 16012–16013.

(24) Felton, G. A. N.; Mebi, C. A.; Petro, B. J.; Vannucci, A. K.; Evans, D. H.; Glass, R. S.; Lichtenberger, D. L. *J. Organomet. Chem.* **2009**, *694*, 2681–2699.

(25) Notice that substitution of carbonyls with cyanide ligands, which are always found in the enzyme active site, is not expected to be functional to enhance the electronic communication between bma and the diiron core. In fact, cyanides are known to negatively shift the redox potential of biomimetic diiron clusters. (see Felton; *J. Organomet. Chem.* **2009**, *694*, 2681–2699.) Results confirming such a picture are reported in the Supporting Information, where the electronic structure of dicyanide complexes derived from **1** is illustrated (complexes $[\mathbf{1(CN)_2}]^{3-}$, $[\mathbf{1(CN)_2\_termH}]^{2-}$, and $[\mathbf{1(CN)_2\_\mu H}]^{2-}$).

(26) Huang, C. S.; Peng, C. C.; Chou, C. H. *Tetrahedron Lett.* **1994**, *35*, 4175–4176. Trahanovsky, W. S.; Miller, D. L.; Wang, Y. L. *J. Organomet. Chem.* **1997**, *62*, 8980–8986. Munzel, N.; Kesper, K.; Schweig, A.; Specht, H. *Tetrahedron Lett.* **1988**, *29*, 6239–6242.

(27) Roseboom, W.; De Lacey, A. L.; Fernandez, V. M.; Hatchikian, E. C.; Albracht, S. P. J. *J. Biol. Inorg. Chem.* **2006**, *11*, 102–118.

(28) Silakov, A.; Kamp, C.; Reijerse, E.; Happe, T.; Lubitz, W. *Biochemistry* **2009**, *48*, 7780–7786.

(29) Yu, L; Greco, C; Bruschi, M; Ryde, U; De Gioia, L; Reiher, M. *Inorg. Chem.* **2011**, *50*, 3888–3900.

(30) Liu, X. F.; Yin, B. S. *J. Coord. Chem.* **2010**, *63*, 4061–4067. Zeng, X. H.; Li, Z. M.; Xiao, Z. Y.; Wang, Y. W.; Liu, X. M. *Electrochem. Commun.* **2010**, *12*, 342–345. de Hatten, X.; Bothe, E.; Merz, K.; Huc, I.; Metzler-Nolte, N. *Eur. J. Inorg. Chem.* **2008**, 4530–4537. Liu, Y. C.; Lee, C. H.; Lee, G. H.; Chiang, M. H. *Eur. J. Inorg. Chem.* **2011**, 1155–1162.

(31) Eilers, G.; Schwartz, L.; Stein, M.; Zampella, G.; de Gioia, L.; Ott, S.; Lomoth, R. *Chem.—Eur. J.* **2007**, *13*, 7075–7084.

(32) Koelle, U.; Infelta, P. P.; Gratzel, M. *Inorg. Chem.* **1988**, *27*, 879–883.